ARTEMIS IV RADIO OBSERVATIONS OF THE 14 JULY 2000 LARGE SOLAR EVENT

C. CAROUBALOS[1], C. E. ALISSANDRAKIS[3], A. HILLARIS[2], A. NINDOS[3],
P. TSITSIPIS, X. MOUSSAS[2], J.-L. BOUGERET[5], K. BOURATZIS[2], G. DUMAS[5],
G. KANELLAKIS[6], A. KONTOGEORGOS[4], D. MAROULIS[1], N. PATAVALIS[1],
C. PERCHE[5], J. POLYGIANNAKIS[2] and P. PREKA-PAPADEMA[2]

[1]*Department of Informatics, University of Athens, GR-15783, Athens, Greece*
[2]*Section of Astrophysics, Astronomy and Mechanics, Department of Physics, University of Athens, GR-15784 Athens, Greece*
[3]*Section of Astro-Geophysics, University of Ioannina, GR-45110 Ioannina, Greece*
[4]*Department of Electronics, Technological Education Institute of Lamia, Lamia, Greece*
[5]*Observatoire de Paris, Département de Recherche Spatial, CNRS UA 264, F-92195 Meudon Cedex, France*
[6]*Thermopylae, O.T.E Inmarsat, GR-35009, Skarpheia, Molos, Greece*

Abstract. In this report we present a complex metric burst, associated with the 14 July 2000 major solar event, recorded by the ARTEMIS-IV radio spectrograph at Thermopylae. Additional space-borne and Earth-bound observational data are used, in order to identify and analyze the diverse, yet associated, processes during this event. The emission at metric wavelengths consisted of broad-band continua including a moving and a stationary type IV, impulsive bursts and pulsating structures. The principal release of energetic electrons in the corona was $15-20$ min after the start of the flare, in a period when the flare emission spread rapidly eastwards and a hard X-ray peak occurred. Backward extrapolation of the CME also puts its origin in the same time interval, however, the uncertainty of the extrapolation does not allow us to associate the CME with any particular radio or X-ray signature. Finally, we present high time and spectral resolution observations of pulsations and fiber bursts, together with a preliminary statistical analysis.

1. Introduction

Radio emission from solar flares can be detected from millimeter to kilometer wavelengths. Flare microwave emission can provide important diagnostics of acceleration processes in the corona because the radio emission is produced by energetic electrons accelerated during the flare. The microwave flare component is broad-band in frequency with no appreciable drift and relatively slowly varying (i.e., with time scales from about tens of seconds up to more than one hour).

At longer wavelengths, flare radio emission shows an extraordinary variety of structure in frequency, time and space, some of which is near or at the limit of our observing facilities. Type III bursts (cf., McLean, 1985, and references therein) appear on the spectrum as intense bands of emission drifting rapidly from high to low frequencies. They are produced as electrons, accelerated at low altitudes, gain

access to open field lines and propagate well out into the corona. Type U bursts on the other hand trace the propagation of energetic electrons along closed magnetic field lines (coronal loops).

Type II bursts represent the passage of a MHD shock wave through the tenuous plasma of the solar corona; their radio emission is due either to energetic electrons accelerated at the shock front or plasma turbulence excited by the shock; they originate either by a flare blast wave or by a CME forward shock (Maia *et al.*, 2000; Aurass, 1997).

The continua observed during periods of activity, on the other hand, represent the radiation of energetic electrons trapped within magnetic clouds, CMEs and plasmoids and they appear under the name type IV bursts. The moving type IV bursts (Boischot, 1957, also dubbed IVmA after Takakura, 1969; see also Slottje, 1981) are emitted from sources of meter wave continuum which are believed to move outwards at velocities of the order of $100-1000$ km s^{-1}; their spectrum is often featureless and they sometimes last more than 10 min. Some of them appear following type II bursts and are possibly caused by energetic electrons produced in the wake of the type II shock. Others originate from energetic electron populations trapped in expanding magnetic arches or plasmoids, i.e., blobs of dense plasma containing their own magnetic field (cf., Wild and Smerd, 1972; Stewart, 1985, and references therein). The moving type IV (IV mA) bursts which are believed to originate within CMEs may be used for the CME detection by radio methods (Aurass, 1997). The stationary type IV bursts (IV mB after Takakura, 1969; see also Slottje, 1981) emanate from stationary sites usually located above active regions (Robinson, 1985). Type IV events present fine structure, such as pulsating structures, fiber bursts and zebra patterns, while much less abundant are spike bursts, braided zebra patterns and the extremely rare tadpole bursts (Slottje, 1981).

In this article we present a preliminary analysis of a complex event that took place on 14 July 2000. It produced a high flux of high-energy particles that reached the Earth (24000 proton flux units, reported by NOAA Space Environment Centre), while the associated solar wind velocity measured by various spacecraft near Earth was about 1000 km s^{-1}. The flare was accompanied by a filament eruption and a coronal mass ejection. A multitude of space-borne and ground-based instruments observed the event in the entire electromagnetic spectrum from kilometric radio waves to hard X-rays. Our analysis is based on observational data obtained with the ARTEMIS-IV multichannel radio spectrograph, studied in conjunction with images from the Nançay radioheliograph as well as data from soft and hard X-ray instruments.

Section 2 presents the observations. The analysis of the data, covering both the global aspects of the burst evolution and the fine structure is presented in Section 3. Discussion and conclusions are given in Section 4.
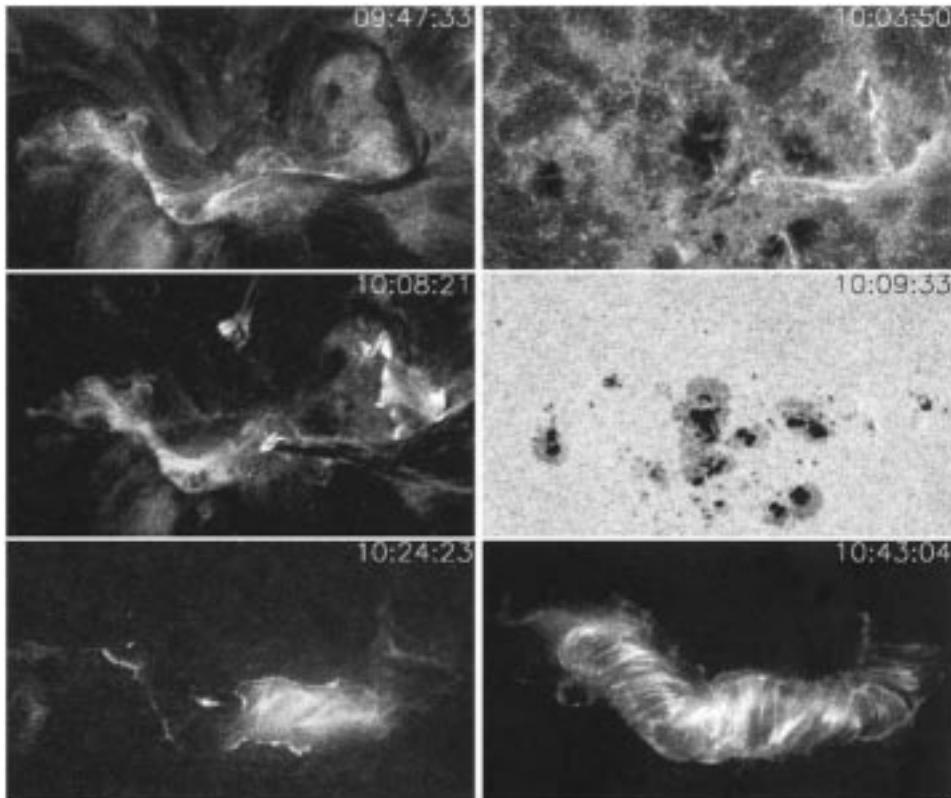
Figure 1. TRACE images before and during the flare. The image at 10:03:50 UT is at 1600 Å, the one at 10:09:33 UT is in white light, the others are at 195 Å.

2. Observations

Our observations were obtained with the ARTEMIS-IV solar radiospectrograph, operating at Thermopylae, Greece (Caroubalos *et al.*, 2001). The instrument covers the frequency range of 110 to 687 MHz, using two receivers operating in parallel. One, the Global Spectral Analyser (ASG), is a sweep frequency receiver and the other, the Acousto-Optic Spectrograph (SAO), is a multichannel acousto-optical receiver. The sweep frequency analyzer covers the full frequency band with a time resolution of 10 samples s^{-1}, while the high-sensitivity multi-channel acousto-optical analyzer covers the 265–450 MHz range, with high frequency and time resolution (100 samples s^{-1}). In the present study we exploit both data sets: The broad band, medium time resolution set of the ASG in order to study the association of spectral features of the event with 2D images from the Nançay radioheliograph (NRH) as well as with data from other instruments and the narrow band, high time resolution SAO mostly for the analysis of the fine temporal and spectral structures.
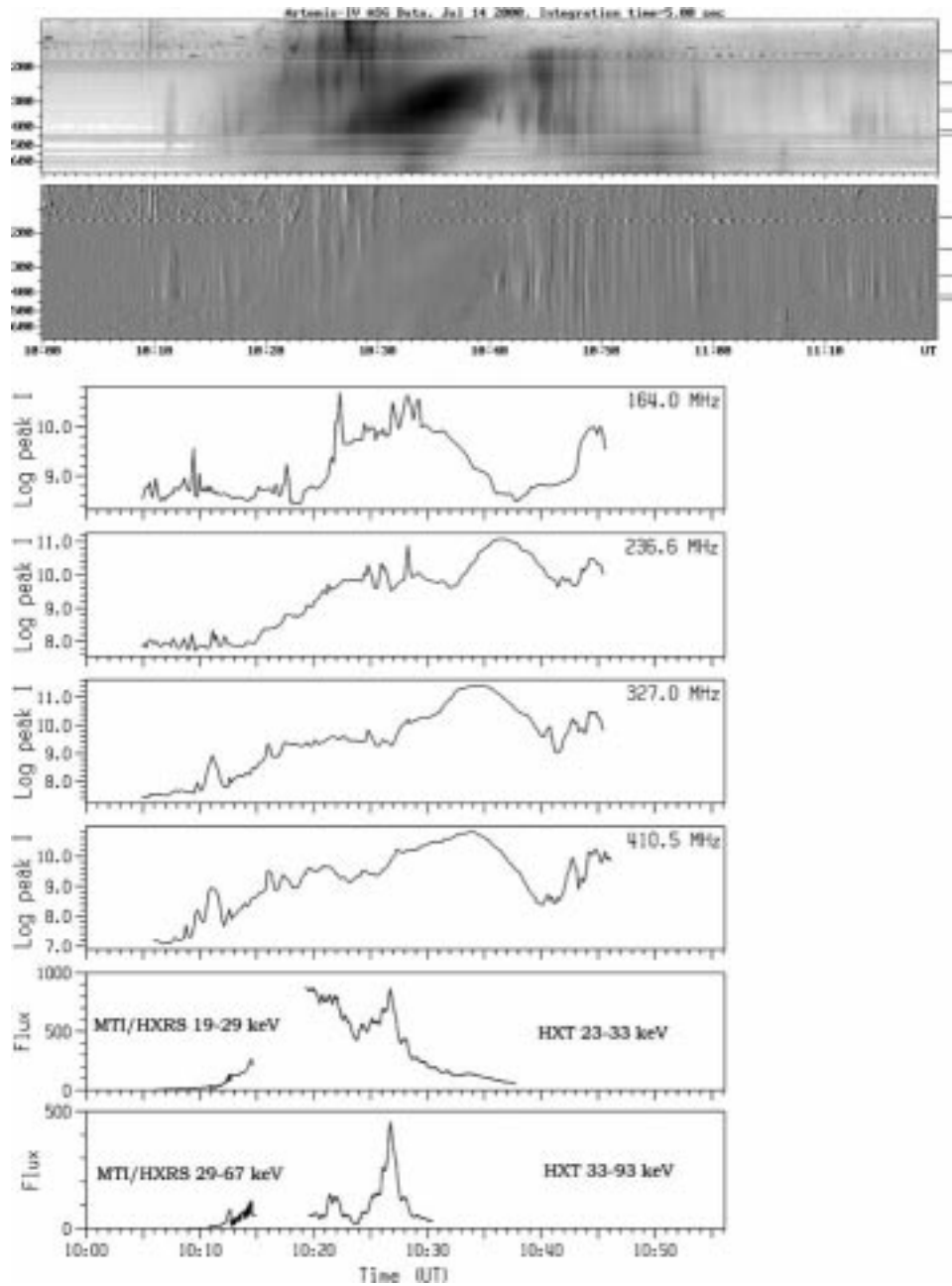
Figure 2. The dynamic spectrum of the event observed with the ARTEMIS-IV ASG receiver (*upper two panels*); the *lower panel* shows the time derivative of the flux, which helps to identify rapidly varying structures. *Horizontal lines* at the right of the spectrum mark the frequencies of the Nançay radioheliograph channels. The four plots below the spectrum give the logarithm of the peak intensity (in K), measured by the NRH at four frequencies. The *lower two panels* show the hard X-ray flux observed with the *Yohkoh* HXT and the MTI HXRS instruments.

The Nançay radioheliograph provides two-dimensional images of the Sun at five frequencies between 450 and 150 MHz with sub-second time resolution (Bonmartin *et al.*, 1983; Kerdraon and Delouis, 1997). For the present study we used images integrated over 10 s, between 10:05:57 and 10:45:27 UT (provided by the Radioheliograph group), at 164, 236.6, 327, 410.5, and 432 MHz; All five frequencies are within the spectral range of the ASG, while the last three are also within the range of the SAO. Radio emission at these frequencies comes from the low and middle corona (height 0.1–0.5 solar radii).

In addition to the Artemis and NRH data, we made use of soft X-ray observations from TRACE (at 195 Å and 1600 Å), GOES and the *Yohkoh* SXT instruments. The hard X-ray data were from the *Yohkoh* HXT and the HXRS aboard MTI (Fárník, Garcia, and Kiplinger, 1998). The former is a Fourier synthesis type imager with 0.5 s time resolution in four energy bands between 14 and 93 keV. The latter is an X-ray spectrometer with 200 ms time resolution in flare mode in the range 12.6 to 250 keV. Finally we used white-light coronograph data from LASCO C2 and C3 coronographs.

3. Results

3.1. OVERVIEW

Descriptions of the event have been given by Zhang *et al.* (2001), Klein *et al.* (2001) and Karlický *et al.* (2001). We summarize here and in Table I the main stages of its evolution, in conjunction with the radio spectral data.

The Hα flare started at 10:03 UT, with a maximum at 10:24, in active region 9077 near the disk center (N17 E01). The GOES flux started to rise at 10:03:06 UT in the 3–25 keV channel and 50 s later in the 1.5–10 keV channel; the maximum was reached at 10:24 UT and the event was classified as X5.7. There is a data gap in the TRACE 195 Å images in the critical time interval between 09:58 and 10:08 UT, therefore we used 1600 Å continuum images in order to detect the flare onset. The first flare kernels were visible in the image at 10:03:50 UT (Figure 1), which is consistent with the GOES data. Before that time there was some activity along the neutral line filament. At 10:08:21 UT the flare ribbons were already well visible in the NW part of the active region, with bright emission between them, apparently from diffuse loops. In the same TRACE image the disrupted filament is clearly seen to rise rapidly and can be followed till about 10:30 UT, silhouetted dark in front of the bright flaring region.

The flare was confined to the west part of the active region until about 10:24 UT, at which time it spread abruptly to the east part (Figure 1). At about the same time distinct fine loop structures joining the flare ribbons became prominent in the west part of the flare, while by 10:40 UT the entire flaring region, both in the west and the eastern part of the region was dominated by a spectacular loop system.
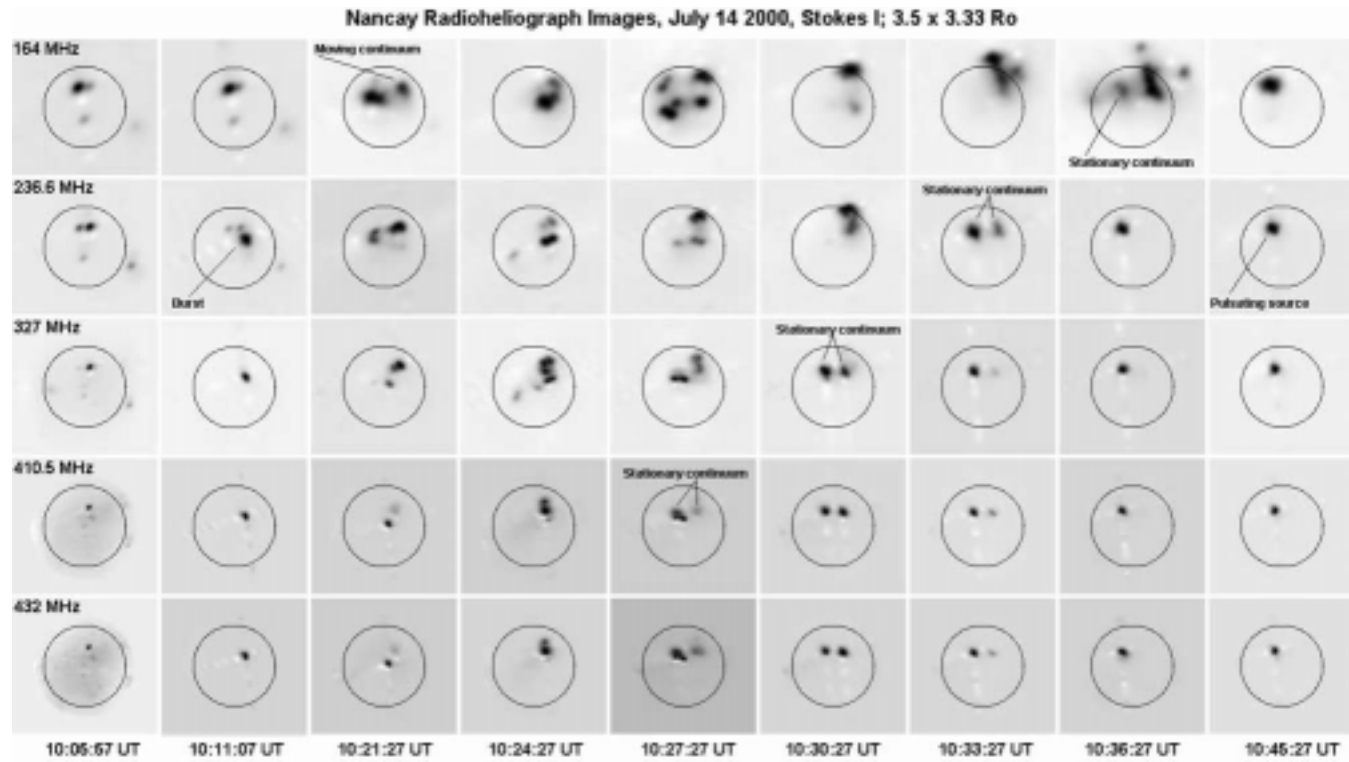
Figure 3. Images at five radio frequencies obtained with the Nançay radioheliograph, illustrating the evolution of the event. Each image row corresponds to a particular frequency and each column to a particular time. The white features are artifacts of the de-convolution, hence only the dark features are considered.
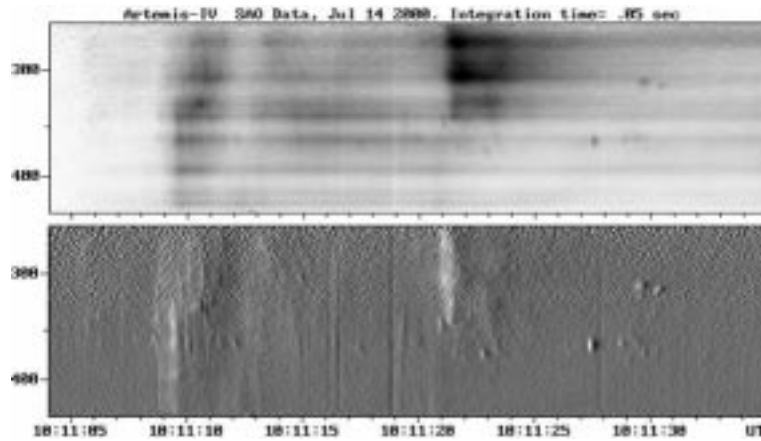
Figure 4. High-resolution dynamic spectrum of the burst shown in the second column of Figure 3, observed with the SAO, in flux (*top*) and differential (*bottom*) displays.

In Figure 2 (lower panels) we present HXT data in the energy range of 23–33 keV and 33–93 keV, combined with MTI/HXRS data in the 19–29, 29–67.2 keV range, respectively. The combined *Yohkoh* HXT and HXRS data leave a gap between 10:15 and 10:19:36 UT, within which apparently a significant part of the hard X-ray emission occurred. After the gap there is a peak at 10:26:45 UT, which is harder than the rest of the observed part of the burst emission and coincides in time with the spread of the flare in the west part of the active region. According to HXT imaging, it consists of two compact components. We could not reliably determine their exact position because they were located outside the SXT field of view, which included only the west part of the flaring region; we can only say that the components were east of the SXT field of view, which brings them close to region where the flare expanded.

The dynamic spectrum of the event, observed with the ASG, is given in the upper panel of Figure 2. The temporal resolution has been reduced to 5 s, in order to provide an overall view of the event. In the same figure we give logarithmic plots of the peak intensity observed with the radioheliograph at four frequencies. Figure 3 presents selected images from the Nançay radioheliograph that, in conjunction with the dynamic spectrum, illustrate the evolution of the event.

The dynamic spectrum shows a complex pattern of emission, which includes impulsive bursts, continua and pulsations. The Radioheliograph Group (Klein *et al.*, 2001) reported noise storms preceding the flare, located near the central meridian in the northern hemisphere (Figure 3, left column). It is interesting to note that there was very little other activity until several minutes after the start of the flare. The group of type III's around 10:09 UT (Figure 2) is *collocated* with the noise storm rather than with the flaring region. Another group of what appear to be fast drift bursts in the ASG spectrum occurred around 10:11:10–10:11:30 UT at frequencies above 210 MHz. The corresponding NRH images are shown in

TABLE I

Major phases of the 14 July event

Time (UT)	Optical and X-rays	Metric radio
10:03	Start of flare in Hα and soft X-rays	Pre-existing noise storms from the N. hemisphere (cf., Figure 3).
10:06		Weak continuum onset at 432 and 411 MHz
10:07:36		Weak continuum onset at 327 MHz (Figure 2)
10:08–10:10		Type III's from the same region in N. hemisphere as the noise storm.
10:08:21	Flare and disrupted filament clearly visible at 195 Å	
10:09:27		Weak continuum onset at 237 MHz
10:11:10		First flare associated drift bursts
10:12		Continuum seen in dynamic spectrum
10:15:37		Weak continuum onset at 164 MHz
~10:18		Start of motion of continuum source
10:20–10:30		Isolated type III and III G's
10:24	Flare maximum (GOES)	
10:24:20	Flare spreads east	
10:26:45	Hard X-ray peak >33 keV	
10:27		Onset of stationary continuum
10:30	Filament last seen at 195 Å	
10:34:00		Continuum peak at 411 MHz
10:34:30		Continuum peak at 327 MHz
10:36:30		Continuum peak at 237 MHz
10:38		Onset of fiber bursts and pulsations
10:41		End of stationary continuum
10:54	Halo CME reaches 5.4 $R_\odot$ in C2 ($v = 1700$ km s^{-1})	
11:42	Halo CME reaches 12.5 $R_\odot$ in C3 ($v = 1000$ km s^{-1})	

Figure 3, second column; they are visible at all NRH frequencies except 164 MHz and are located near the flare. For comparison, we give in Figure 4 the dynamic spectrum of this event with 50 ms time resolution, observed with the SAO. The high-resolution observations reveal considerable fine structure and practically no frequency drift of the individual components.

Impulsive bursts, including a type III storm as well as short-scale time variations, became more frequent in the time interval 10:20 to 10:30 UT, gradually
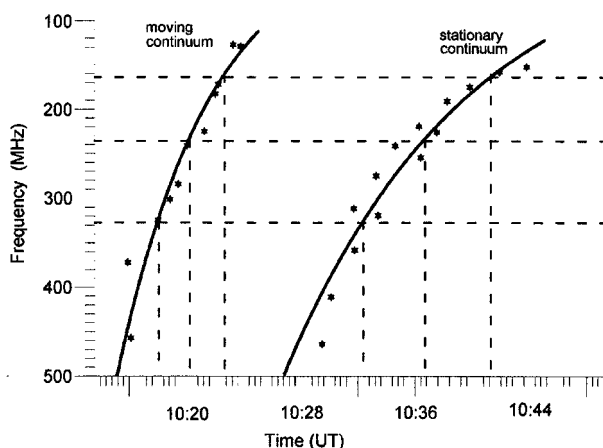
Figure 5. Position of maxima of the type II and type IV mA as a function of frequency (linear scale) and time. Both are fitted with exponential curves (*solid lines*). *Horizontal dashed lines* mark the 164, 236.6, and 327 MHz levels of NRH, *vertical lines* mark the time at which each continuum crosses the corresponding layer.
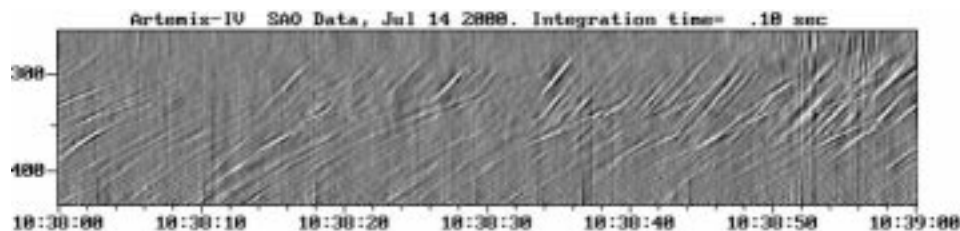

Figure 6. Time derivative of the dynamic spectrum observed with the SAO over a one minute interval in the 265–441 MHz range.

drifting to lower frequencies (Figure 2). It is interesting to note that they occurred around the time of the hard X-ray peak (10:26:45 UT) and the spread of the flare in the east part of the active region. Therefore it appears that, before this time, very few energetic particles could find their way to the corona, although such particles were released in the lower atmosphere as evidenced by the hard X-ray emission.

The fast drift bursts coexist with a faint type II burst, which in the dynamic spectrum became prominent around 10:11 UT at high frequencies and was detectable until about 10:27 UT at the low frequency end of the ASG band (Figure 2). Even before 10:11, continuum emission appeared at 10:06 UT in the 432 and 410.5 MHz NRH images, as a localized source at the west side of the flaring region. This emission became later visible at 327 MHz ($\sim$ 10:07:37 UT), at 236.6 MHz ($\sim$ 10:09:27 UT) and finally at 164 MHz ($\sim$ 10:15:37 UT); clear evidence for its existence and progressive appearance from high to low frequencies is provided by the logarithmic NRH intensity time curves of Figure 2.

The position of the continuum peak on the dynamic spectrum is shown in Figure 5 (left curve). Although its drift rate is within the range of type II bursts, it had

too large a bandwidth and lacked fine spectral structure. This slow-drift continuum was practically stationary until about 10:18 UT, when part of the emission started moving north, in the form of a moving type IV (Klein *et al.*, 2001; cf. Figure 3, columns 3–6).

The most prominent feature of the dynamic spectrum is a broad, structureless continuum, apparently a type IV, which started around 10:27 UT and extended above 1.5 GHz (see Figure 10 of Karlický *et al.*, 2001). Although it shows a clear frequency drift (Figure 5, right curve) it was associated with two stationary sources (Figure 3, columns 5–8), one located west and the other east of the active region. The western source faded around 10:35, while the eastern source persisted until 10:41 UT and was followed by pulsations, which originated at the same location (Figure 3, last column). The pulsations show a very complex temporal/spectral structure in the ASG spectrum, while they are much better visible in the SAO spectrum (see next section). They appear at frequencies above 150 MHz and persisted until about 11:30 UT.

The flare was accompanied by an Earth-directed halo coronal mass ejection (CME). The analysis of the SOHO coronagraph (C2, C3) images shows that the velocity of the CME, estimated on the plane of the sky, was about 1800 km s^{-1}, with lower and upper limits of 1660 and 1900 km s^{-1} respectively. The large expansion velocity of the CME between 5.4 and 9.4 $R_\odot$ (Table I) might be attributed to errors of estimation of the extent of the CME, but it is also possible that an acceleration of the CME by the vast number of particles injected by the explosive phenomena during this time period took place.

Backwards extrapolation of the CME position, on the basis of the measurements given in Table I, shows that the CME exploded near 10:23:20 UT (±7.5 min). Whatever the value of this raw estimate, it gives evidence that the origin of the CME is associated with the enhanced activity in the interval 10:20–10:30 UT described above, although it is impossible from this information alone to establish its association with and of the metric radio components.

3.2. FINE STRUCTURE

Due to its high sensitivity, spectral and temporal resolution, the SAO is ideal for studies of fine temporal structure, such as the one following the moving type IV bursts. In this section we present examples of such structures, together with a preliminary analysis.

A one minute long dynamic spectrum in the interval 10:38 to 10:39 UT is shown in Figure 6; what is actually shown is the time derivative of the flux, which eliminates any underlying continuum emission and enhances fast varying structures. The most prominent feature in the spectrum is the fine, drifting bursts (fiber bursts) of ~ 300 ms duration. They appear at frequencies above 280 MHz and at least two families with different drift rates coexist.
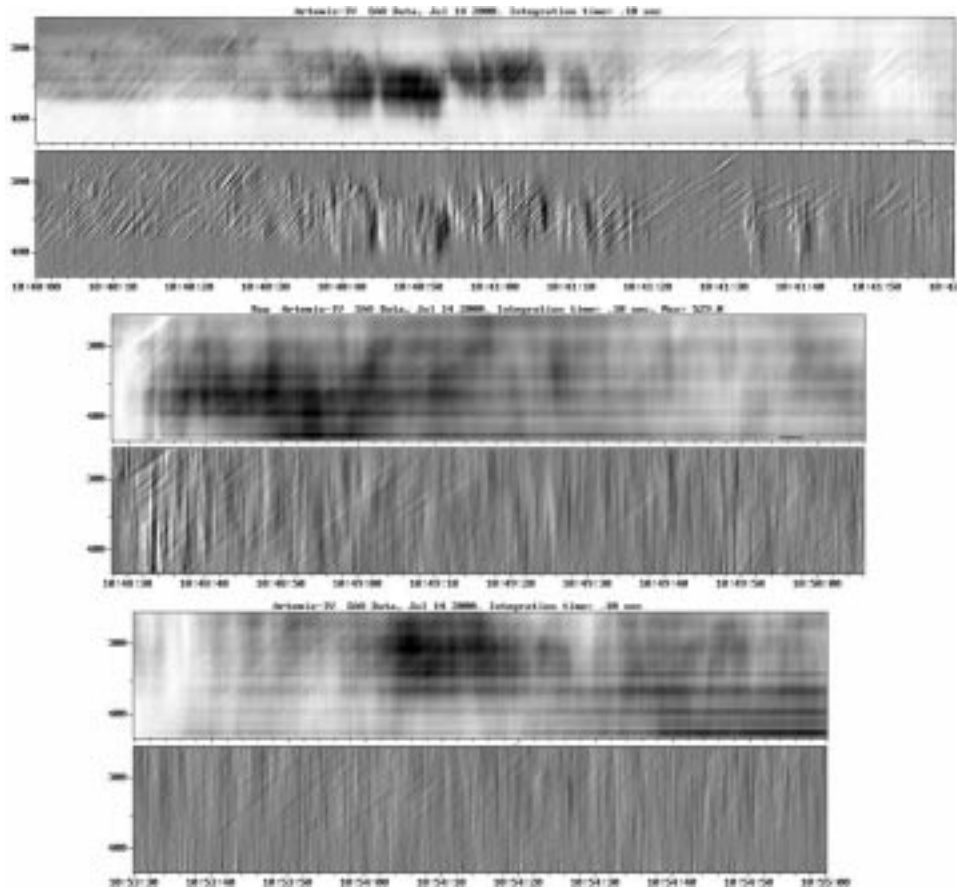
Figure 7. Dynamic spectra of fiber bursts and pulsations (flux and its time derivative) during the late stage of evolution of the event.

Three more examples are shown in Figure 7, at different periods during the late stages of evolution of the event. Both the flux and its time derivative are shown; in the flux spectrum, the average value has been subtracted in order to better show the fine structure.

The top spectrum shows a mixture of fiber bursts and pulsations, in the interval 10:40–10:42 UT. The fiber bursts have similar characteristics as those of Figure 6; the pulsations, with periods of ~ 200 ms, were limited to the spectral range 290–410 MHz, and appeared in groups. Later in the event (second spectrum in Figure 7), the pulsations became more numerous and extended beyond the 265–445 MHz SAO band; they became the predominant feature still later (third spectrum of Figure 7).

We are in the process of developing numerical methods for studying the statistical properties of the numerous fine features seen in the spectra. We have already developed a feature tracking algorithm, on the basis of which we can compute the
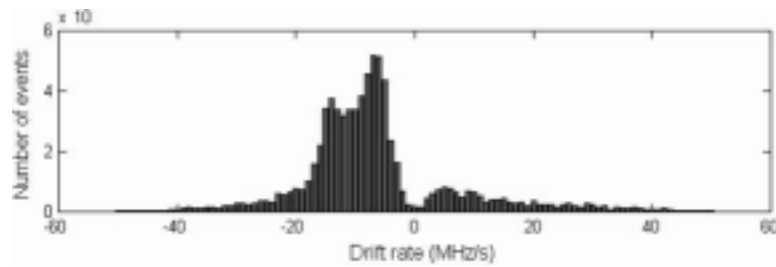
Figure 8. Distribution of drift rates during the interval of 10:38–10:39 UT (cf., Figure 6).

distribution of the drift rates of fiber bursts. An example is shown in Figure 8, where we give the histogram of drift rates for the same interval as in Figure 6. As expected, most features show negative frequency drifts and the two fiber burst families of Figure 6 are discernible, associated to histogram peaks at -6 and -12 MHz s^{-1}; the histogram also shows a few reverse (positive) drift structures.

4. Summary and Conclusions

The event of 14 July 2000 is typical of a large flare, manifesting itself in all possible ways. The flare produced complex metric radio emission, with several components: impulsive, continua and pulsations. Imaging data from the Nançay radioheliograph, used in conjunction with spectral data from Artemis-IV, facilitated their identification.

Although the flare started at 10:03 UT in Hα and soft X-rays, it was the time interval 10:18 to 10:30 that was the most rich in phenomena, including a faint type II, a moving type IV followed by a stationary type IV, a hard X-ray peak and a rapid expansion of the flare eastwards. It also appears that during this period most of the energetic electrons were released in the corona, as evidenced by the multitude of fast drift bursts. Backwards extrapolation of the CME position measured on LASCO C2 and C3 images also points to this time interval for the origin of the CME, although its association with any particular feature of the radio emission is not clear.

The metric emission was also rich in pulsating structures and fiber bursts, which followed the type IV burst and lasted for more than one hour. We presented a preliminary statistical analysis of fiber bursts, that reveals two co-existing families with different drift rates. We are in the process of improving our analysis and we expect to present more thorough results in the near future.

Acknowledgements

References

Aurass, H.: 1997, in G. Trotted (ed.), 'Coronal Physics from Radio and Space Observations', *Proceedings of the CESRA Workshop 3-7 June 1996, Lecture Notes in Physics* **483**, 135.

Boischot, A.: 1957, *Compt. Rend. Acad. Sci.* **244**, 1326.

Bonmartin, J., Bouteille, A., Clavelier, B., Issartel, M. P., Kerdraon, A., Lantos, M. F., Lantos, P., Mercier, C., Pick, M., Raoult, A.: 1983, *Solar Phys.* **88**, 383.

Caroubalos, C., Maroulis, D., Patavalis, N., Bougeret, J-L., Dumas, G., Perche, C., Alissandrakis, C., Hillaris, A., Moussas, X., Preka-Papadema, P., Kontogeorgos, A., Tsitsipis, P., and Kanellakis, G.: 2001, *Exp. Astron.* **11**, 23.

Fárník, F., Garcia, H., and Kiplinger, A.: 1998, *CESH Conference, ESA*, Noordwijk, p. 305.

Karlický, M., Yan, Y., Fu, Q., Wang, S., Jiřička, K., Mészárosová, H., and Liu, Y.: 2001, *Astron. Astrophys.* **369**, 1104.

Kerdraon A. and Delouis J.-M.: 1997, In G. Trotted (ed.), 'Coronal Physics from Radio and Space Observations', *Proceedings of the CESRA Workshop 3-7 June 1996, Springer Lecture Notes in Physics* **483**, 192.

Klein, K.-L., Trottet, G., Lantos, P., and Delabourdiniere, J.-P.: 2001, *Astron. Astrophys.* **373**, 1073.

Maia, D., Pick, M., Vourlidas, A., and Howard, R.: 2000, *Astrophys. J.* **528**, L49.

McLean, D. J.: 1985, in D. J. McLean and N. Labrum (eds.), *Solar Radiophysics*, Cambridge University Press, Cambridge, p. 37.

Robinson, R. D.: 1985, in D. J. McLean and N. Labrum (eds.), *Solar Radiophysics*, Cambridge University Press, Cambridge, p. 385.

Slottje, C.: 1981, *Atlas of Fine Structures of Dynamic Spectra of Solar Type IV-dm and Some Type II Radio Bursts. N.F.R.A Dwingeloo and Astronomical Institute of Utrecht*, Utrecht.

Stewart, R. T.: 1985, in D. J. McLean and N. Labrum (eds.), *Solar Radiophysics*, Cambridge University Press, Cambridge, p. 361.

Takakura, T.: 1969, in C. de Jager and Z. Švestka (eds.), *COSPAR: Solar Flares and Space Research*, p. 165.

Wild, J. P. and Smerd, S. F.: 1972, *Ann. Rev. Astron. Astrophys.* **10**, 159.

Zhang, J., Wang, J., Deng, Y., and Wu, D.: 2001, *Astrophys. J.* **548**, L99.